Environmental Research 167 (2018) 453–467

Contents lists available at ScienceDirect

Environmental Research

journal homepage: www.elsevier.com/locate/envres

Projected monthly temperature changes of the Great Lakes Basin

Liang Zhang[a,b,*], Yingming Zhao[a,b], David Hein-Griggs[c], Jan J.H. Ciborowski[a]

[a] Department of Biological Sciences, University of Windsor, 401 Sunset Avenue Windsor ON N9B 3P4, Canada
[b] Aquatic Research and Development Section, Ontario Ministry of Natural Resources and Forestry, 301 Milo Road, Wheatley, ON, Canada N0P 2P0
[c] University of Exeter, Prince of Wales Road, Exeter EX4 4SB, United Kingdom

ARTICLE INFO

Keywords:
Monthly temperature
Tmax and Tmin
Fluctuations of latitudinal temperature gradients
Great Lakes Basin

ABSTRACT

The Great Lakes Basin is an important agricultural region for both the United States and Canada. The regional crop growths are affected by inter-annual climatic conditions and intra-seasonal variability. Consequently, monthly climate change projection data can provide more useful information for crop management than seasonal climate projections. However, very few studies undertaken for the Great Lakes Basin have focused on monthly timescales. In this study, we investigate the projected mid-century (2030–2059) monthly mean maximum temperature (Tmax) and minimum temperature changes of this region, relative to the baseline period (1980–2009). Future Tmax increases in this region are likely to be greater during the May to October period (coinciding with the region's growing season) than in other months. The order of magnitude of future Tmax and Tmin changes of the five Great Lakes sub-basins are Superior > Huron > Michigan > Erie and Ontario. Most future Tmax changes over land areas are higher than those over the lakes, whereas Tmin changes are likely to be higher over lakes than over the adjacent land areas in this region. The future number of extreme warm days (Tmax ≥ 29–32 °C) in this region will increase by between about 5 days (in the north) to 40 days (in southern parts of the basin), while the number of winter cold days (Tmax ≤ −5 °C ~ 0 °C) may decrease by between 3 days (south) and 35 days (north). This study furthermore identifies some fluctuations of latitudinal temperature gradients in the Great Lakes Basin, these areas covering the north latitude 40.5–41.5°, 43.5–44.0°, 45.5–46.5°, and 47.5–49.5°.

1. Introduction

The Laurentian Great Lakes Basin is important to the economies and societies of both the United States and Canada. This region comprises over 20% of the world's surface freshwater (80% of North America's freshwater resources), not only providing drinking water to over 33 million people (10% of the US and 30% of the Canadian population), but also supporting the huge industrial and agricultural sectors of the two countries (Kling et al., 2003; Wuebbles et al., 2010). Agriculture in the Great Lakes Basin is important for both the US and Canada, accounting for approximately 7% and 25% of the total US production and Canadian production, respectively (USEPA, 2008). In Canada, Ontario farms provide jobs for 1.4 million people and account for $9.1 billion in annual revenues. Food processing companies in Ontario also generate 120,000 jobs and $32.5 billion in annual revenues (OMAFRA, 2016). Corn and soybeans are the two largest planted crops in this region.

Temperature is a very important factor affecting plant growth. In a recent corn growth experiment in Iowa US, the corn yield of the chamber under normal temperature was 471.2 g/m^2, but the corn yield of the controlled chamber (mean temperature increased 4 °C) declined sharply to 59.9 g/m^2 (Hatfield and Prueger, 2015). Prior to that, based on the historical (1976–2006) crop production for the US state of Wisconsin, Kucharik and Serbin (2008) found that both corn and soybean yield trends were enhanced in counties that experienced a trend towards cooler and wetter conditions during the summer. They also suggested that for each additional degree (1 °C) of future warming during summer months, corn and soybean yields could potentially decrease by 13% and 16%, respectively. Based upon the national climate and crop data, Schlenker and Roberts (2009) reported increases in crop yields (1950–2005) in the United States as a function of temperature increases up to 29 °C for corn, 30 °C for soybeans, and 32 °C for cotton. However, those crops yields sharply decreased when temperature increased beyond these thresholds. A study of historical (1965–2008) corn production in Northeast China (latitudes similar to those in the Great Lakes basin) showed that the corn yield was significantly correlated with the daily minimum temperature in May and September (Chen et al., 2011).

* Corresponding author at: Department of Biological Sciences, University of Windsor, 401 Sunset Avenue, Windsor, ON, Canada N9B 3P4.
E-mail addresses: Liang.Zhang@uwindsor.ca, zhang.on.ca@gmail.com, zhangliang07_08@163.com (L. Zhang).

https://doi.org/10.1016/j.envres.2018.08.017
Received 24 May 2018; Received in revised form 22 July 2018; Accepted 10 August 2018
Available online 11 August 2018

The temperature optimum of different crops (including corn and soybean) varies among different growing stages during the between April and November in North America (Neild and Newman, 1987; Hatfield and Prueger, 2015; Andresen, 2017). For example, the two, four and six corn leaf fully emerged stages need an accumulated 200, 345 and 475 growing degree days (GDDs), respectively. Attainment of the corn kernels dented and physiological maturity stages require a total of 2450 and 2700 GDDs, respectively (Neild and Newman, 1987). These studies indicated that crop growth estimates rely on knowledge of monthly temperature variation rather than estimates of seasonal temperature variation. Similarly, a recent study on six Wisconsin (US) lakes (Winslow et al., 2017) also revealed that seasonal temperature changes could not fully represent the effects of climate change on lake temperatures change, and suggested that monthly temperature changes should be a proxy for seasonal patterns. Clearly, projected monthly temperatures data could provide more detailed and reliable information than the seasonal temperature patterns (e.g. Gula and Peltier, 2012; Wang et al., 2016) for agricultural management in practice.

The HadCM3Q Perturbed Physics Ensemble (PPE) of GCMs is a version of the United Kingdom Met Office Hadley Centre's third generation coupled ocean-atmosphere general circulation model HadCM3, in which the Great Lakes are explicitly represented by the model (Wilson et al., 2010). This allows the HadCM3Q GCMs to simulate interactions between the atmosphere and surface of the Great Lakes more realistically than using a non-flux corrected GCM alone. The PRECIS (Providing REgional Climates for Impacts Studies) regional climate modeling (RCM) system was developed by the Hadley Centre (Jones et al., 2004). It can generate high-resolution climate change information for any region of the world, thus providing detailed projections of climate (Jones et al., 2004; Massey et al., 2015). PRECIS has been applied to regions throughout the world, many of which encompass large expanses of both land and water (e.g. the Caribbean (Campbell et al., 2011), Southeast Asia (McSweeney et al., 2012), the Mediterranean and Middle East (Constantinidou et al., 2016)). Other studies have investigated regions adjacent to large water bodies (e.g. the Pacific Northwestern United States, Zhang et al., 2009).

In this study, we use PRECIS to downscale selected HadCM3Q GCMs. The objective is to project and compare mid-century (2030–2059) monthly temperature (Tmax and Tmin) with a baseline period (1980–2009), with an additional focus on understanding how Tmax and Tmin will change over land areas and the lake surfaces.

2. Methods

The HadCM3Q perturbed physics ensemble contains 17 GCMs. Individual GCMs are named HadCM3Q0, HadCM3Q1, HadCM3Q2, HadCM3Q3 and so on up to HadCM3Q16 (Wilson et al., 2010; McSweeney et al., 2012). The external forcing in the HadCM3Q PPE are according to the Special Report on Emissions Scenarios (SRES) A1B emissions scenario (Wilson et al., 2010), and the water-surface boundary conditions are taken directly from the water component of the HadCM3Q0 GCM model (Wilson et al., 2010).

PRECIS is a comprehensive model that considers both the water and land surface components of the climate system. It can represent important physical processes within the climate system, such as dynamic flow, the atmospheric sulfur cycle, clouds and precipitation, radiative processes, and the interactions between land surface and deep soil (Jones et al., 2004; Massey et al., 2015). PRECIS can downscale at two resolutions: $0.44 \times 0.44^{\circ}$ (about $50\,km \times 50\,km$) and $0.22 \times 0.22^{\circ}$ (about $25\,km \times 25\,km$) (Wilson et al., 2010). A previous study had revealed that five HadCM3Q GCMs (HadCM3Q0, Q3, Q10, Q13, and Q15) span most of above mentioned 17 GCMs parameters (McSweeney et al., 2012). In this study, we downscale five GCMs (HadCM3Q0, Q3, Q10, Q13, and Q15) with PRECIS at $25\,km \times 25\,km$ resolution to project future Great Lakes Basin climate changes for the mid-century (2030–2059). The various physical configurations of the five GCMs (Table 1) enable us to estimate uncertainties in the climate change projections that arise from GCMs parametrization. We chose a baseline period of 1980–2009 for this study. All the projections of future climate differences are expressed as the future period (2030–2059) estimates minus the baseline period (1980–2009).

The Mann-Kendall trend test (Mann, 1945; Kendall, 1975) and Sen's slope (Sen, 1968) have been widely used to quantify the significance of trends and changing rates in hydro-meteorological time series, respectively (Gocic and Trajkovic, 2013). To assess the historical temperatures changing trends of the 16 sites, we calculated the Mann-Kendall Z values and Sen's slopes of the temperature series (Tmean, Tmax, and Tmin) of the 16 weather stations (upon the observation data between 1980 and 2009).

3. Results and discussions

3.1. Data validation

To validate the performance of PRECIS simulation, we chose eight Canadian weather stations and eight US weather stations (Fig. 1) from the two countries' long-term weather observation networks. We obtained daily climate data from the 16 stations for comparison with the PRECIS results generated over the same baseline period (1980–2009). The locations of the 16 stations encompassed the whole basin and were situated on land areas adjacent to lakes (Duluth MN, Flint ON, Chicago IL, Toronto ON, Cleveland OH, etc.) and the bordering landmass of the lakes (Lansing MI, Sudbury ON, Ottawa ON, etc.), allowing us to assess the models' performance (five GCMs and PRECIS) in capturing the land and water variations across this region.

Comparisons for monthly mean Tmax, Tmean, and Tmin of observed versus output data from five simulations are shown in Fig. 2. Most (46 in 48) observations fell within the range of simulated results, except for Tmin at Flint and Wawa stations. Point to point data validations may yield gaps at some sites, but the overall performance of the simulation should be considered on a large scale as in previous studies (Vavrus and Van Dorn, 2010; Wang et al., 2016), because no climate simulations could accurately (100%) project all single sites (grids) climate in practice.

In Table 2, we compared our simulation performance with other recently published climate simulation data validations that focused on (or involved) this region. The data validation biases (-0.9 °C to +0.7 °C) in this study are comparable to (or smaller than) the biases (-2 °C to +1.93 °C) in recent studies despite different downscaling methods (statistical and dynamical) (Vavrus and Van Dorn, 2010; Gao et al., 2012; Gula and Peltier, 2012; d'Orgeville et al., 2014; Notaro et al., 2015). The data validations indicate the models we selected could do well in simulating the temperature variations of the Great Lakes Basin. Because the historical data observed from 16 stations represent the climate results reflecting the complex land-lake interactions and closely match the data simulations for the validation portion of this study, we

Table 1
Selected parameters of the five different GCMs physics configurations used in this study.

	HadCM3Q0	HadCM3Q3	HadCM3Q10	HadCM3Q13	HadCM3Q15
V_{f1} (ms^{-1})	1	1.32784	0.50546	1.52212	1.71394
C_t (s^{-1})	1.0e-4	0.000337	0.000329	0.000273	7.4e-5
C_w_land ($kg\,m^{-3}$)	0.0002	0.000169	0.00172	0.000985	0.00017
C_w_water ($kg\,m^{-3}$)	5.0e-5	4.07e-5	0.00043	0.000246	4.1e-5
Water-ice diffusion coefficient ($m^2\,s^{-1}$)	2.5e-05	2.387e-5	2.393e-5	2.433e-5	2.347e-5
Boundary layer flux profile parameter	10	12.4727	8.6838	7.2765	12.8178
Ice particle size (um)	30	28.249	29.069	33.348	30.078
Charnock constant	0.012	0.0121	0.0157	0.0123	0.0162

** V_{f1}- Ice fall speed, C_t - Cloud droplet to rain conversion rate, C_w - Cloud droplet to rain conversion threshold, Charnock constant - Roughness lengths and surface fluxes over water. More details of other parameters can be found in Murphy et al. (2004) and Collins et al. (2006).

Fig. 1. Location of the study area (Great Lakes basin) within North America, and the sixteen stations selected for data validation.

are confident that the simulations also effectively represent the temperature variations that are affected by the interactions between land and large water bodies. The key point in Great Lakes basin (and other regions that include both land and large water bodies) climate projection should be to accurately simulate the interactions between lakes and their adjacent land areas (as opposed to considering lakes and lands separately). A model approach in which downscaling a GCM that represents both the lakes and the land has more internal consistency (and less uncertainty) than an approach by which separate land and lake models were used because, each additional exoteric model used could reduce the model consistency between lands and lakes in the projection results (e.g. Gula and Peltier, 2012; Notaro et al., 2015). Our data validation results (Table 2) also demonstrate that the climate projections with GCMs which consider land and lake data in a single model (such as PRECIS in this study), may be preferable to previous projection that simulating land and lake data from different land climate model and lake climate model (Gula and Peltier, 2012; d'Orgeville et al., 2014; Notaro et al., 2015).

We calculated the Mann-Kendall Z values and Sen's slopes of the temperature series (Tmean, Tmax, and Tmin), which based the 16 stations 30-year observation data (1980–2009) and shown in Table 3. The results of the Mann-Kendall analyses indicated that at least one temperature variable (Tmean, Tmax, or Tmin) exhibited statistically significant increases ($p < 0.05$) in September at most stations (13 in 16 stations; Table 3). Overall, the most significant changes were observed between June and September. The Toronto weather station data even showed significant increases in each month from June to November (Table 3). The Mann-Kendall trend test and Sen's estimations also indicated that Tmin and winter temperatures increased more quickly at stations on the Canadian side of the Great Lakes than on the US site. However, the temperature changes also varied from station to station.

Additionally, the Sen's slope estimations showed the Tmin at some

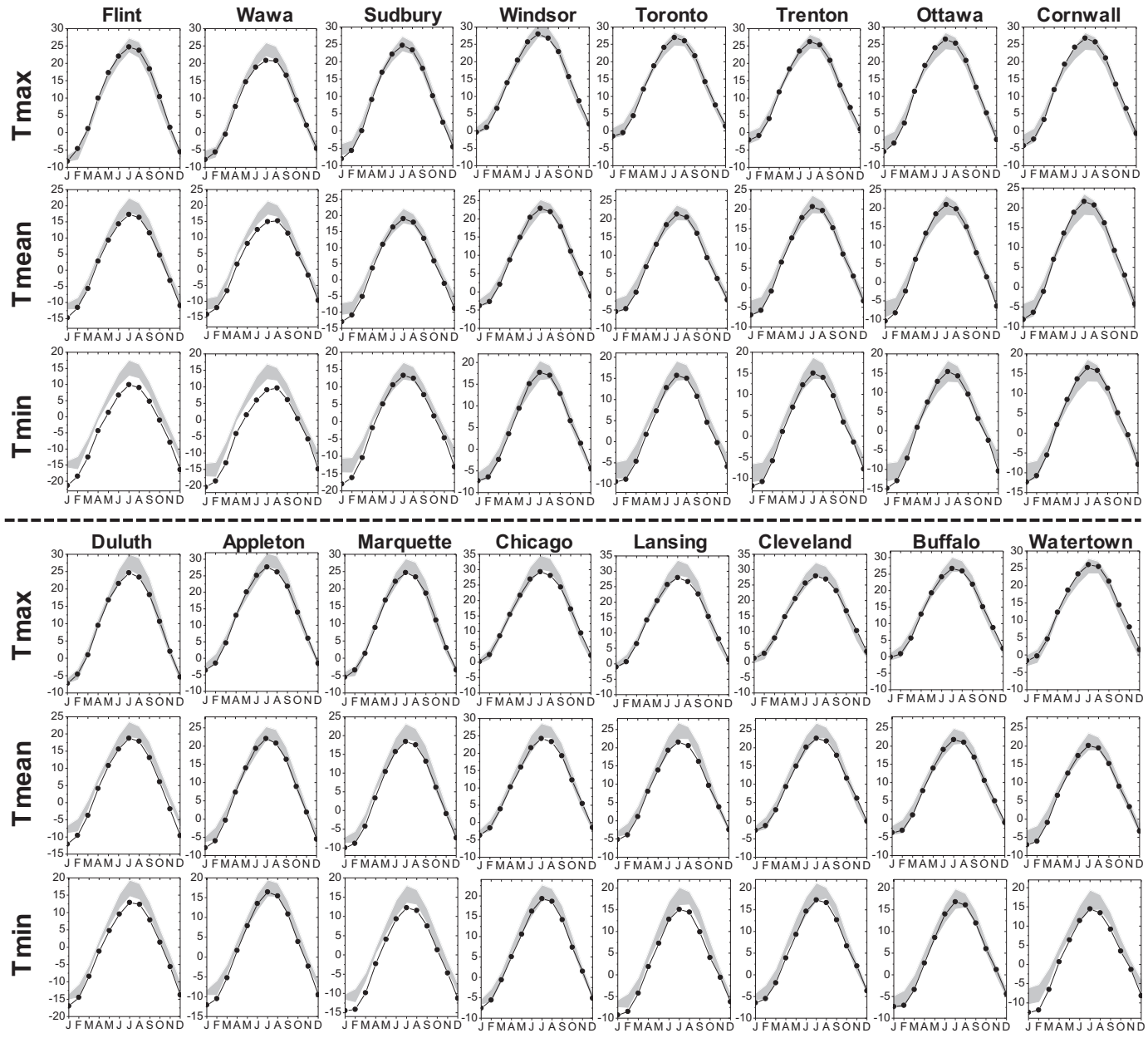

Fig. 2. The sixteen site point-to-point temperature (Tmax, Tmean, and Tmin) validations between observations and PRECIS simulating results upon the baseline period (1980–2009). The upper and lower panels represent the 8 Canadian sites and 8 US sites, respectively. Black dots are observation data, and shaded areas show the PRECIS simulation results.

stations (Flint and Wawa in Canada, Duluth, Appleton, Marquette, and Watertown in the US) have decreased between February and August over the past 30 years (even though only one station (Appleton) significantly decreased in July, Table 3). Some local stations temperatures are also affected by local terrains (mountain, waterside, airport, etc.), but most climate change models simulate the temperature changing with relative smooth tendencies (compared with observations). The Sen's slope estimations also partly explained why some stations' simulated Tmin were higher than the observation data (Fig. 2). Overall, the data validation, Mann-Kendall trend test, and Sen's slope estimations demonstrate the good performance of the PRECIS and the five GCMs we chose in this study.

3.2. Future monthly Tmax and Tmin changes in the basin

Basin-wide maps of the distribution of future monthly mean Tmax

Table 2
The data validation comparisons (biases that "simulated result" minus "referred data") between this study and recent Great Lakes basin climate studies. "Sta_obs" means the station historical weather observation dataset.

Study	GCMs	Downscaling method	Resolution	Studied area	Referred data	Compared period	Compared data scales	Model biases ("Simulated result"- "referred data")	
								Summer Tmax (°C)	Winter Tmin (°C)
This study	HadCM3Q series (Q0, Q3, Q10, Q13, Q15) GFDL,	Dynamical (PRECIS)	25 × 25 km^2	16 cities	Sta_obs	1980–2009	point to point[a]	−0.9 to 0.7	-0.4 to 3.7
				16 cities	Sta_obs	1980–2009	Mean 16 sites[a]	0.2	1.2
				CA 8 cites	Sta_obs	1980–2009	CA 8 sites[a]	0.2	1.2
				US 8 cites	Sta_obs	1980–2009	US 8 sites[a]	0.1	1.2
Vavrus and Van Dorn, 2010		Statistical (mean of 3 GCMs)	Point to Point	Chicago	Sta_obs	1980–2010	point to point[a]	0.7	0.4
	HadCM3, PCM			Chicago	Sta_obs	1961–1990	point to point	1.0	0.3
Gao et al. (2012)	CESM 1.0	dynamical (WRF)	4 × 4 km^2	Michigan	NCDC	2001–2004	State	1.93	n/a
	CESM 1.0	dynamical (WRF)	4 × 4 km^2	Ohio	NCDC	2001–2005	State	0.68	n/a
	CESM 1.0	dynamical (WRF)	4 × 4 km^2	New York	NCDC	2001–2006	State	0.78	n/a
Gula and Peltier (2012)	CCSM3	dynamical (WRF)	10 × 10 km^2	GLs basin	CRU	1979–2001	Broader GLs basin	± 1.26	± 1.20
d'Orgeville et al. (2014)	CCSM3	dynamical (WRF)	10 × 10 km^2	GLs basin	CRU	1979–1994	Broader GLs basin	Tmean[b] = -1 to −2	
Notaro et al. (2015)	MIROC5	dynamical (RegCM4)	25 × 25 km^2	GLs basin	UOD	1980–1999	Broader GLs basin	Tmean[b] = ± 1.9	
	CNRM	dynamical (RegCM4)	25 × 25 km^2	GLs basin	UOD	1980–2000	Broader GLs basin	Tmean[b] = ± 1.16	

Note: The names of GCMs, RCMs and published data (NCDC, CRU, UOD) in this table abbreviated, due to the limited space here. The abbreviations are commonly used in climate studies, and details can be found in the according references and our study (HadCM3Q and PRECIS).
The underlined data scales mean the data were averaged value of the certain entries in this table. Note: The broader areas included, the calculated biases will be less, because the large biases could be averaged/covered by other small biases.

[a] This study model biases showed in this table are the least-biased simulated results, details can be found in Tables 1, 2, 3.

[b] The extreme wet day bias in reference (Vavrus and Van Dorn, 2010) represents the precipitation > 50 mm/day, but our extremely wet day in our study is defined as ≥ 40 mm/day.

and Tmin increases are presented in Figs. 3 and 4, respectively. The five experiments showed the five GCMs downscaled by PRECIS generate different monthly temperature projections (Figs. 3 and 4) due to their different formulations. However, the five simulations exhibited some consistent variations: 1) The smallest temperature (Tmax and Tmin) increases occur during the month of April; 2) future summer (June to September) temperature (Tmax and Tmin) increases in the south/southwest (US) are larger than those in the north (Canada) part in the region; 3) future winter (December to March) temperature (Tmax and Tmin) increases in the south (US) will be smaller than those in north/northeast (Canada) portions of the region; 4) future Tmax increases in this region are likely to be greater in May to October (the majority of the growing season for crops in the region) than in other months.

Crop yields are affected by the interactive effects of climate and management changes (Twine and Kucharik, 2009). The US Corn Belt corn yields have increased in the past decades in most places between 1981 and 2015. However, if the factor of cultivars changes is excluded (which accounts for about 265 of the yield increases), US Corn Belt corn yield actually declined by 12.6 bushels/acre (Sacks and Kucharik, 2011). Median corn planting dates in the US Corn Belt had advanced about 10 days (50% planted Julian day from 132 to 122) from 1981 to 2005, and soybean planting dates advanced by about 12 days (50% planted Julian day from 152 to 140) in that period. The corn growth period (from planting to maturity) was extended by 10 days between 1981 and 2005 (Sacks and Kucharik, 2011). The US Michigan Agricultural Statistics (2012–2016) also showed that the median planting date of corn and soybeans had started at April 20 and April 30, respectively, and the corn and soybean harvest dates could be reached by December 10 and November 30, respectively (Andresen, 2017). Another study on Great Lakes Basin frost-free periods also showed the last spring frost day and first fall frost day have advanced by 5 days and delayed by 7.5 days between 1980 and 2010, respectively (Yu et al., 2014). All of these studies showed that earlier crop planting is a widespread trend in agricultural management in this region of North America. However, due to the large size of the water bodies (Great Lakes), effects on the ambient temperature of the adjacent land, the land areas' first frost-free dates were always 10–30 days later than those over the Great Lakes (Yu et al., 2014). The results of our study indicate that in the future, April will exhibit the lowest annual temperature increase (Figs. 3 and 4), suggesting that farmers' strategy of planting crops earlier in the year (Sacks and Kucharik, 2011) may be of limited value in this region in future, mostly due to the Great Lakes' influence. The projected continuously greater warming between May and October relative to other months could stimulate crop growth of the crop on one hand but may be harmful to the crops' productions during days on which Tmax exceeds 32 °C (Schlenker and Roberts, 2009).

To knowledge, this may be the first study to investigate the Great Lakes Basin future monthly temperature changes, although some previous studies have examined seasonal climate change projections (Gula and Peltier, 2012; d'Orgeville et al., 2014; Notaro et al., 2015; Wang

Table 3
The 16 stations (8 Canadian and 8 US sides) historical (1980–2009) temperature series (Tmean, Tmax, and Tmin) trend analysis results (Bold Z value with asterisk ($|Z| > 1.96$) present the trend is statistically significant ($p < 0.05$) in Mann-Kendall analysis, the Sen's slope unit is ℃ /year).

	Flint_CA						Wawa_CA					
	MK trend (Z value)			Sen's slope			MK trend (Z value)			Sen's slope		
	Tmean	Tmax	Tmin	Tmean	Tmax	Tmin	Tmean	Tmax	Tmin	Tmean	Tmax	Tmin
Jan	1.021	0.563	0.855	0.078	0.055	0.133	0.946	0.517	0.660	0.077	0.040	0.100
Feb	0.688	0.813	0.396	0.058	0.100	0.050	− 0.244	− 0.281	− 0.225	− 0.016	− 0.034	− 0.009
Mar	0.125	1.126	− 0.646	0.007	0.050	− 0.036	0.019	0.732	− 0.469	0.000	0.037	− 0.018
Apr	0.396	0.146	− 0.438	0.014	0.021	− 0.020	0.125	0.303	− 0.232	0.005	0.017	− 0.010
May	− 1.042	− 1.105	− 0.750	− 0.044	− 0.048	− 0.038	− 0.375	− 0.428	− 0.161	− 0.013	− 0.023	− 0.006
Jun	1.438	1.668	1.376	0.076	0.100	0.056	**2.569** *	**2.319** *	**2.855** *	0.100	0.086	0.116
Jul	0.396	0.813	− 0.271	0.007	0.033	− 0.005	0.785	− 0.089	**2.034** *	0.028	− 0.008	0.050
Aug	1.001	**1.961** *	− 0.250	0.044	0.100	− 0.011	0.357	0.161	0.624	0.014	0.005	0.020
Sep	**2.447** *	**3.152** *	0.838	0.095	0.153	0.045	**3.564** *	**3.583** *	**3.039** *	0.118	0.127	0.100
Oct	0.855	1.564	− 0.125	0.027	0.071	0.000	1.267	0.856	**2.105** *	0.050	0.033	0.067
Nov	1.480	1.376	1.105	0.096	0.096	0.090	1.820	0.946	**2.319** *	0.082	0.061	0.127
Dec	**2.147** *	**2.251** *	**1.962** *	0.200	0.175	0.231	1.160	1.106	1.356	0.100	0.092	0.143
	Toronto_CA						Trenton_CA					
	MK trend (Z value)			Sen's slope			MK trend (Z value)			Sen's slope		
	Tmean	Tmax	Tmin	Tmean	Tmax	Tmin	Tmean	Tmax	Tmin	Tmean	Tmax	Tmin
Jan	1.392	1.178	1.320	0.100	0.070	0.108	0.825	1.013	0.769	0.085	0.085	0.083
Feb	0.535	0.446	0.714	0.030	0.031	0.036	0.225	0.319	− 0.150	0.016	0.015	− 0.014
Mar	1.302	0.803	1.463	0.048	0.040	0.056	0.300	0.657	− 0.019	0.006	0.030	0.000
Apr	1.332	0.882	1.763	0.044	0.040	0.050	0.161	0.714	− 0.553	0.000	0.029	− 0.013
May	0.321	− 0.464	0.928	0.008	− 0.020	0.038	− 0.535	− 0.571	− 0.803	− 0.017	− 0.013	− 0.021
Jun	**3.086** *	1.534	**3.996** *	0.105	0.071	0.147	**2.819** *	1.784	**2.872** *	0.080	0.075	0.100
Jul	1.070	− 0.178	**2.409** *	0.033	− 0.011	0.067	− 0.339	− 0.731	0.196	− 0.009	− 0.021	0.000
Aug	**1.963** *	1.320	**2.819** *	0.064	0.043	0.094	0.999	1.570	0.785	0.025	0.043	0.025
Sep	**3.451** *	**2.814** *	**3.902** *	0.100	0.100	0.119	**2.284** *	**2.944** *	**1.534** *	0.064	0.100	0.041
Oct	1.838	1.219	**2.964** *	0.075	0.041	0.095	0.856	0.517	1.516	0.033	0.020	0.050
Nov	**2.026** *	1.801	**2.307** *	0.074	0.070	0.076	1.632	**1.970** *	1.407	0.060	0.080	0.050
Dec	0.803	0.428	0.981	0.050	0.025	0.071	0.413	0.244	0.619	0.039	0.022	0.051
	Duluth_US						Appleton_US					
	MK trend (Z value)			Sen's slope			MK trend (Z value)			Sen's slope		
	Tmean	Tmax	Tmin	Tmean	Tmax	Tmin	Tmean	Tmax	Tmin	Tmean	Tmax	Tmin
Jan	0.624	0.303	0.731	0.052	0.024	0.076	0.119	0.237	0.178	0.000	0.022	0.007
Feb	0.107	0.036	− 0.339	0.006	0.000	− 0.030	− 0.844	− 0.844	− 0.188	− 0.039	− 0.042	− 0.024
Mar	0.178	0.250	− 0.089	0.008	0.018	− 0.008	− 0.810	− 0.514	− 1.205	− 0.045	− 0.038	− 0.073
Apr	− 0.071	− 0.446	0.517	0.000	− 0.013	0.018	− 0.393	0.018	− 1.338	− 0.020	0.000	− 0.052
May	− 1.142	− 1.516	− 0.410	− 0.043	− 0.073	− 0.013	− 1.726	− 1.932	− 1.763	− 0.092	− 0.100	− 0.085
Jun	1.160	0.303	**2.212** *	0.033	0.014	0.061	− 0.056	− 0.169	0.169	0.000	− 0.007	0.005
Jul	− 0.553	− 0.624	0.161	− 0.007	− 0.029	0.000	− 1.688	− 1.163	**− 2.739** *	− 0.061	− 0.050	− 0.069
Aug	0.642	0.375	0.268	0.019	0.020	0.008	− 0.675	0.450	− 1.407	− 0.021	0.015	− 0.054
Sep	**3.140** *	**3.176** *	**2.605** *	0.100	0.100	0.093	1.225	**2.173** *	0.138	0.043	0.092	0.005
Oct	1.088	1.534	1.017	0.043	0.046	0.050	0.393	1.017	− 0.321	0.017	0.040	− 0.007
Nov	1.374	1.213	1.017	0.088	0.080	0.082	1.426	1.613	0.769	0.070	0.098	0.035
Dec	1.285	1.035	1.570	0.084	0.064	0.100	0.469	0.732	0.506	0.033	0.037	0.046
	Lansing_US						Cleveland_US					
	MK trend (Z value)			Sen's slope			MK trend (Z value)			Sen's slope		
	Tmean	Tmax	Tmin	Tmean	Tmax	Tmin	Tmean	Tmax	Tmin	Tmean	Tmax	Tmin
Jan	0.803	0.821	0.910	0.050	0.045	0.064	1.409	1.285	1.231	0.089	0.067	0.093
Feb	0.357	0.410	0.125	0.011	0.027	0.013	0.535	0.125	0.482	0.029	0.015	0.022
Mar	0.517	0.500	0.535	0.017	0.021	0.031	0.178	− 0.214	0.678	0.008	− 0.007	0.024
Apr	1.070	1.392	0.553	0.036	0.053	0.021	1.338	0.981	1.748	0.045	0.040	0.057
May	− 0.375	− 1.106	0.232	− 0.011	− 0.055	0.016	0.125	− 0.464	0.696	0.008	− 0.012	0.033

(*continued on next page*)

Table 3 (*continued*)

Jun	1.088	0.678	1.838	0.035	0.018	0.063	1.302	0.232	**2.284** *	0.043	0.000	0.067
Jul	− 1.356	− 0.839	− 1.285	− 0.038	− 0.026	− 0.037	− 0.178	− 1.035	0.767	− 0.010	− 0.033	0.017
Aug	− 0.196	− 0.196	− 0.143	− 0.006	− 0.005	0.000	0.856	0.000	1.624	0.033	0.000	0.060
Sep	1.285	1.552	0.464	0.039	0.057	0.017	1.249	0.821	1.624	0.033	0.027	0.040
Oct	0.714	0.303	1.053	0.020	0.018	0.039	0.107	− 0.446	0.910	0.005	− 0.021	0.036
Nov	1.124	0.731	1.320	0.045	0.036	0.044	0.589	0.464	1.195	0.029	0.020	0.036
Dec	0.178	− 0.018	0.428	0.005	0.000	0.021	0.268	0.196	0.589	0.017	0.008	0.029

	Sudbury_CA						Windsor_CA					
	MK trend (Z value)			Sen's slope			MK trend (Z value)			Sen's slope		
	Tmean	Tmax	Tmin	Tmean	Tmax	Tmin	Tmean	Tmax	Tmin	Tmean	Tmax	Tmin
Jan	0.863	0.713	0.863	0.062	0.064	0.076	0.981	0.946	1.035	0.075	0.067	0.078
Feb	− 0.196	− 0.107	− 0.161	− 0.016	− 0.009	− 0.013	0.619	0.769	0.263	0.041	0.038	0.020
Mar	0.769	1.257	0.244	0.038	0.054	0.022	0.750	0.319	0.657	0.029	0.013	0.029
Apr	0.375	0.500	0.214	0.021	0.021	0.005	1.748	1.624	1.213	0.055	0.063	0.037
May	− 0.482	− 0.589	− 0.214	− 0.022	− 0.025	− 0.011	0.089	− 0.357	0.553	0.007	− 0.014	0.021
Jun	**2.409** *	**2.212** *	**2.748** *	0.087	0.077	0.100	**2.026** *	1.069	**2.907** *	0.066	0.041	0.083
Jul	− 0.999	− 1.570	− 0.303	− 0.020	− 0.048	− 0.005	0.263	− 0.019	0.619	0.005	0.000	0.014
Aug	− 0.143	0.089	− 0.428	0.000	0.000	− 0.013	1.053	0.981	1.534	0.030	0.018	0.045
Sep	**2.623** *	**3.015** *	**2.105** *	0.093	0.112	0.075	**2.194** *	1.516	**2.444** *	0.060	0.067	0.069
Oct	0.963	0.696	1.534	0.043	0.033	0.050	0.678	0.357	1.195	0.031	0.010	0.061
Nov	1.392	1.035	1.481	0.064	0.050	0.068	1.659	1.160	1.641	0.052	0.044	0.056
Dec	0.882	0.769	1.163	0.087	0.050	0.102	0.375	0.188	0.450	0.024	0.008	0.036

	Ottawa_CA						Cornwall_CA					
	MK trend (Z value)			Sen's slope			MK trend (Z value)			Sen's slope		
	Tmean	Tmax	Tmin	Tmean	Tmax	Tmin	Tmean	Tmax	Tmin	Tmean	Tmax	Tmin
Jan	0.807	0.825	0.825	0.080	0.071	0.082	0.767	0.892	0.803	0.085	0.055	0.071
Feb	0.036	0.268	− 0.303	0.000	0.017	− 0.022	1.284	1.719	0.632	0.079	0.105	0.038
Mar	− 0.250	0.000	− 0.339	− 0.011	0.000	− 0.018	− 0.036	0.321	− 0.321	0.000	0.008	− 0.014
Apr	0.375	0.624	− 0.161	0.017	0.029	− 0.006	0.500	0.428	0.089	0.014	0.014	0.000
May	− 0.642	− 0.500	− 0.696	− 0.017	− 0.020	− 0.021	− 0.244	− 0.281	0.225	− 0.006	− 0.006	0.008
Jun	1.873	1.659	**2.319** *	0.061	0.058	0.067	**2.284** *	1.713	**2.730** *	0.060	0.055	0.060
Jul	− 0.856	− 1.160	− 0.250	− 0.018	− 0.033	− 0.006	0.750	0.094	1.426	0.018	0.000	0.028
Aug	0.678	0.839	0.250	0.018	0.025	0.009	1.369	1.257	1.369	0.038	0.039	0.037
Sep	**2.194** *	**2.426** *	1.713	0.071	0.100	0.039	**2.837** *	**3.140**	**2.105** *	0.088	0.122	0.065
Oct	0.946	0.482	0.910	0.028	0.017	0.033	1.035	0.874	1.178	0.038	0.044	0.031
Nov	1.669	1.820	1.257	0.067	0.087	0.052	**2.457** *	**2.776**	**2.120** *	0.086	0.113	0.065
Dec	0.394	0.431	0.131	0.033	0.037	0.007	0.581	0.338	0.469	0.042	0.013	0.052

	Marquette_US						Chicago_US					
	MK trend (Z value)			Sen's slope			MK trend (Z value)			Sen's slope		
	Tmean	Tmax	Tmin	Tmean	Tmax	Tmin	Tmean	Tmax	Tmin	Tmean	Tmax	Tmin
Jan	0.571	− 0.232	1.356	0.052	− 0.011	0.100	0.892	0.714	0.910	0.056	0.033	0.073
Feb	− 0.321	− 0.375	− 0.125	− 0.014	− 0.033	− 0.011	0.839	0.446	0.999	0.042	0.038	0.056
Mar	− 0.125	0.107	− 0.339	0.000	0.004	− 0.013	0.075	− 0.657	0.525	0.000	− 0.033	0.027
Apr	0.268	0.000	− 0.107	0.016	0.000	− 0.007	0.600	0.263	0.694	0.022	0.013	0.028
May	− 1.017	− 1.624	− 0.303	− 0.037	− 0.080	− 0.013	− 0.394	− 0.807	0.000	− 0.033	− 0.047	0.000
Jun	1.588	1.213	1.731	0.050	0.040	0.067	0.517	− 0.714	1.695	0.018	− 0.027	0.058
Jul	− 0.821	− 1.231	0.089	− 0.023	− 0.054	0.000	− 0.214	− 0.946	0.642	− 0.007	− 0.039	0.024
Aug	0.250	1.195	− 0.642	0.009	0.039	− 0.022	0.446	− 0.624	**2.105** *	0.019	− 0.030	0.060
Sep	**3.194** *	**3.069** *	**2.765** *	0.100	0.111	0.093	1.677	0.696	**2.498** *	0.050	0.020	0.075
Oct	1.231	0.589	1.659	0.050	0.030	0.071	0.393	− 0.339	1.606	0.013	− 0.017	0.060
Nov	1.142	0.642	1.534	0.064	0.045	0.079	0.957	0.769	1.820	0.053	0.045	0.075
Dec	0.803	0.553	1.088	0.060	0.035	0.074	0.071	− 0.161	0.553	0.000	− 0.006	0.018

(*continued on next page*)

Table 3 (*continued*)

	Buffalo_US						Watertown_US					
	MK trend (Z value)			Sen's slope			MK trend (Z value)			Sen's slope		
	Tmean	Tmax	Tmin	Tmean	Tmax	Tmin	Tmean	Tmax	Tmin	Tmean	Tmax	Tmin
Jan	0.981	0.856	0.946	0.060	0.057	0.075	0.678	0.910	0.517	0.075	0.073	0.067
Feb	− 0.054	0.036	− 0.178	− 0.010	0.000	− 0.016	− 0.071	0.214	− 0.785	− 0.006	0.010	− 0.052
Mar	0.000	− 0.285	0.071	0.000	− 0.008	0.000	− 0.482	− 0.535	− 0.589	− 0.025	− 0.021	− 0.024
Apr	0.107	− 0.018	− 0.446	0.000	0.000	− 0.009	− 0.143	0.624	− 1.231	− 0.005	0.029	− 0.036
May	− 0.731	− 0.803	− 0.839	− 0.035	− 0.027	− 0.029	− 0.938	− 0.657	− 1.351	− 0.025	− 0.027	− 0.043
Jun	1.659	1.017	**2.212** *	0.044	0.036	0.058	**2.157** *	**2.176** *	1.820	0.071	0.077	0.051
Jul	− 0.946	− 1.516	− 0.535	− 0.029	− 0.057	− 0.015	0.000	− 0.356	0.672	0.000	− 0.008	0.019
Aug	0.393	0.268	0.963	0.013	0.006	0.021	0.642	1.249	0.393	0.017	0.044	0.013
Sep	1.945	1.748	1.927	0.050	0.054	0.050	1.427	**2.569** *	0.268	0.045	0.075	0.011
Oct	0.143	− 0.731	0.981	0.000	− 0.025	0.033	0.303	− 0.410	0.571	0.017	− 0.013	0.017
Nov	1.178	0.946	1.017	0.040	0.044	0.033	1.213	1.285	0.678	0.037	0.063	0.025
Dec	0.000	− 0.125	− 0.036	− 0.004	− 0.006	0.000	0.232	0.250	0.250	0.022	0.019	0.022

Note: Due to the limited space (page width) to show all results in this table, we didn't highlight the Mann-Kendall trends at the 1% significance level (while |Z| value > 2.58) with ** here.

et al., 2016). As we have summarized in the introduction, seasonal climate change estimates may not provide enough information to accurately forecast crop growth in a certain region.

3.3. The sub-basins' Tmax and Tmin changes over land and lake areas

The future monthly mean Tmax and Tmin changes of the five sub-basins are shown in Figs. 5 and 6, respectively. The projected magnitude of Tmax and Tmin increases (from greatest change to least amount of change) are Superior > Huron > Michigan > Erie and Ontario, with little difference between the Erie and Ontario sub-basins. The monthly patterns show that April Tmax and Tmin increases will be the smallest in future years over land and lakes, except Tmax over the land in the Lake Superior basin (May). All monthly Tmax and Tmin values are projected to increase by over 2.5 °C between May and October annually, and Tmax increases over lakes are consistently largest in August (Figs. 5 and 6). Nevertheless, the Tmax increases over the land areas are projected to be higher between July and October than in other months (Fig. 5), and projected Tmin increases over Lake Superior basin are greater from January and March than other months (Fig. 6). The differences in general Tmax and Tmin increases over land are greater than those over lakes (bottom plots of Fig. 5), whereas the greatest Tmin increases are likely to occur over lakes than over the land (bottom plots of Fig. 6). These projected results highlight the strong lake effects exerted on the ambient land area climate change in this region.

The projected summer temperature increases over lakes were higher than those over the land areas in summer, but conversely in winter months, these tendencies are similar to previous historical observational studies over lakes Superior, Huron, and Michigan (Austin and Colman, 2007), Moreover, the projected temperature increases (Tmax and Tmin) were greater over the larger sub-basins (Superior, Huron, Michigan) than over the smaller sub-basins (Erie and Ontario), accurately corroborating that larger lakes (water bodies) have more powerful effects on ambient land air temperatures than do smaller lakes (Scott and Huff, 1996; Austin and Colman, 2007; Yu et al., 2014). Those findings in this study not only further verified the effective performance of the models (five GCMs and PRECIS) we selected in this study, but also demonstrate that the Great Lakes continue to strongly influence the ambient land area climate in the future. The detailed monthly temperature projections provided in this study could be used for agricultural management planning of the individual sub-basins for applications such as adjusting the crop planting dates in April and May, and in anticipating which cultivars might best tolerate the higher temperatures projected in August.

3.4. Future cold and extreme warm days in this region

Because US national data has shown the high-temperature thresholds of corn, soybean and cotton growth were 29 °C, 30 °C and 32 °C, respectively (Schlenker and Roberts, 2009), we used the Tmax ≥ 29 °C, 30 °C, 32 °C as the parameters/thresholds by which to identify future extreme warm days in this study. The observed winter (December, January, February) mean Tmax between 1951 and 1980 over most land areas this region were recorded between −5 °C and + 1 °C (Fig. 4 in Scott and Huff, 1996), so we chose the Tmax ≤ 0 °C, −1 °C, −2 °C, −3 °C, −4 °C and −5 °C as the parameters/thresholds by which to project future cold days changes in this study. The projected extreme warm and cold days changes are presented in Figs. 7 and 8. Among the five different GCMs, the results project the number of extremely warm days (Tmax ≥ 29–32 °C) in this region increase by between 5 days (north) and 40 days (south) (Fig. 7), and the number of winter cold days (Tmax ≤ 0 °C ~ −5 °C) could be reduced by between 3 days (south) and 35 days (north) in the future (Fig. 8).

As indicated above, historical observations (Fig. 2) and monthly projection results (Figs. 3–6) had indicated that July and August are the

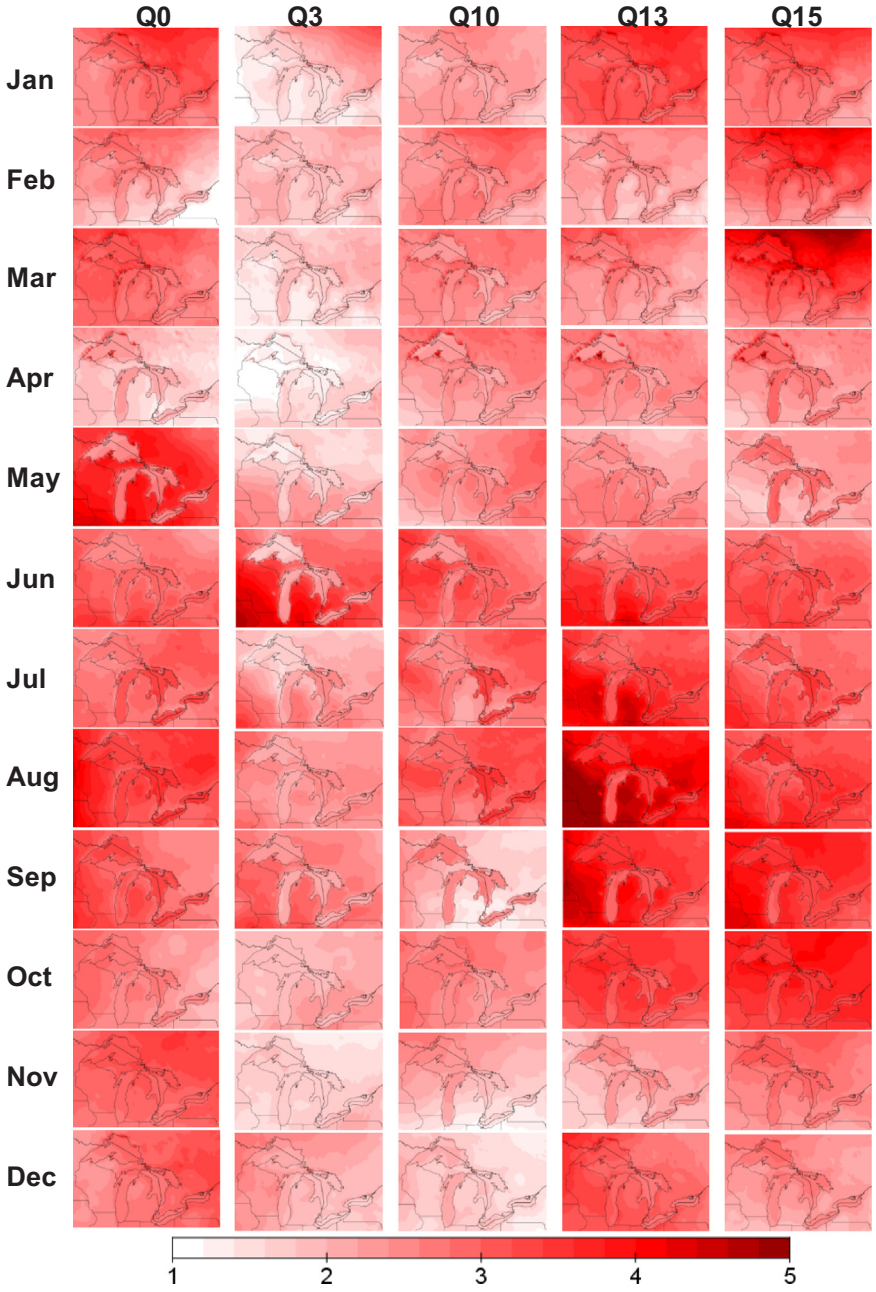

Fig. 3. Projected future (2030–2059) monthly Tmax (°C) changes relative to the baseline period (1980–2009) based upon the five PRECIS experiments.

hottest months annually, and in the future Augusts will be the month likely to exhibit the greatest increases in temperature. Accordingly, the months with the greatest increase of extremely warm days (Fig. 7) will likely be July and August. The corn pollination, silk and kernel dent stages in this region are mainly concentrated in July and August (Andresen, 2017), These three stages are the most important growing stages and are sensitive to temperature extremes (Hatfield and Prueger, 2015). Our results indicate that future corn production in the southern areas of this region may be greatly influenced by the increasing number of extremely warm days, including important US corn states such as Iowa, Wisconsin, Illinois, Michigan, Indiana, and Ohio. However, the future warming may benefit the crop growth on the Canadian side of the Great Lakes basin, especially the lands to the north of Lake Ontario (Fig. 8). However, the milder winter temperatures could promote

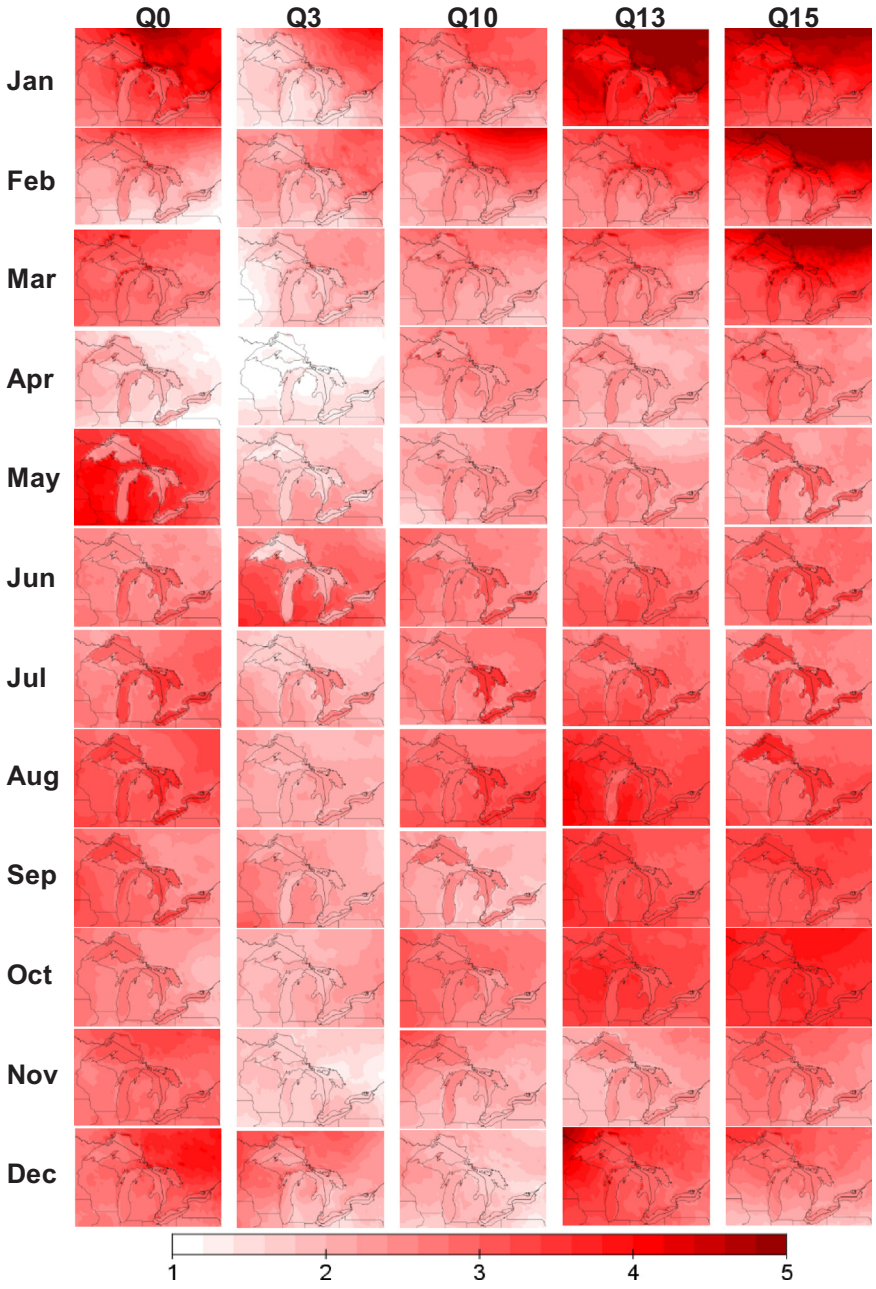

Fig. 4. Projected future (2030–2059) monthly Tmin (°C) changes relative to the baseline period (1980–2009) based upon the five PRECIS experiments.

survival insects injurious to crops in this region, which are normally killed by very cold weather (Gregg et al., 2012). Overall, the future extremely cold days warm days will have varying effects across the Great Lakes basin. Accordingly, farmers on the two sides (Canada and US) may use different strategies (e.g. new cultivars, adjusting planting dates and pest control) to adapt to the warming future.

3.5. Latitudinal fluctuations responded to future warming in this region

In the present study, we calculated estimates for all of the land-dominated areas/grids of this region (bounded by north latitude 39.5–50.0°, and west longitude 93.5–75.5°) and calculated how the increasing number of warm days and decreasing number of cold days varied as a function of latitude (bottom panels in Figs. 7 and 8) across the five experiments. We found that fluctuations in latitudinal temperature gradients in this region, with some variations in the different GCMs (Fig. 9). The results show that the projected increasing numbers of warm days and decreasing numbers of cold days vary according to latitudinal ("Λ" shapes for warm days, "V" shapes for cold days) other than the smooth changes throughout the basin

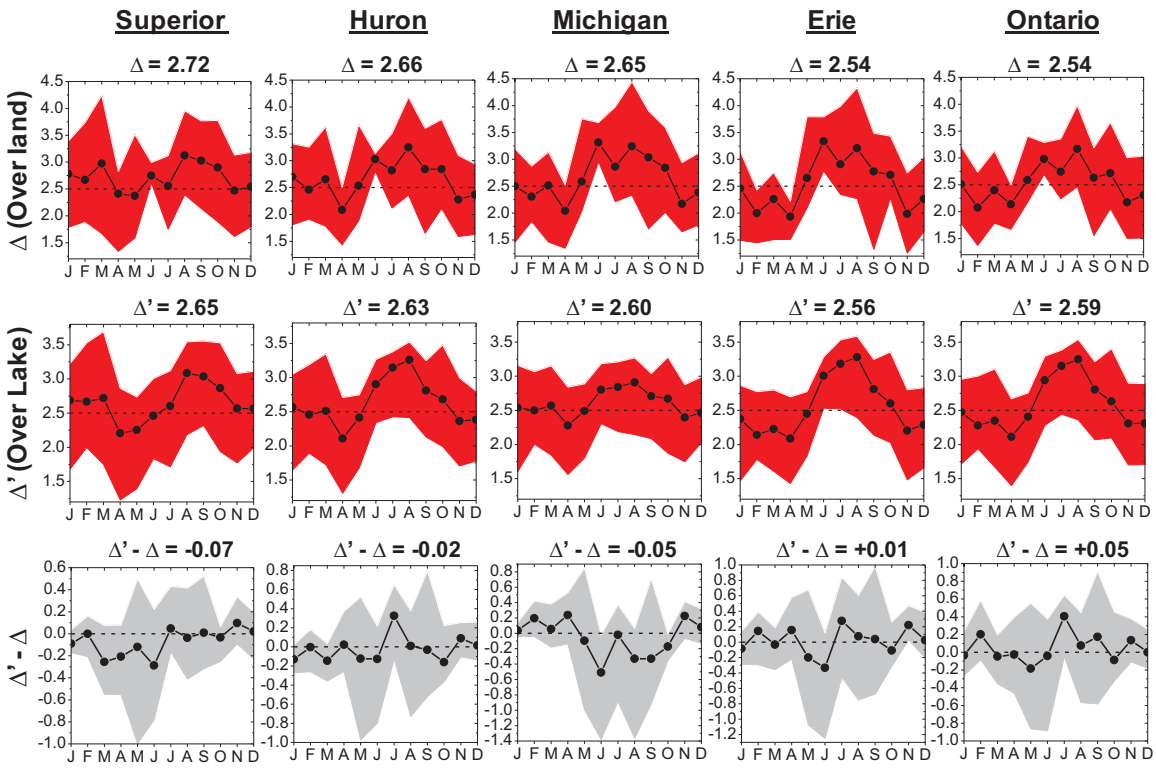

Fig. 5. Projected monthly Tmax increases in the five Great Lakes sub-basins in mid-century (2030–2059). Δ and Δ′ represent the averaged air temperature Tmax changes over land and over lake relative to the baseline period (1980–2009), respectively. "Δ′ - Δ" shows the Tmax change gaps between over lake and over land.

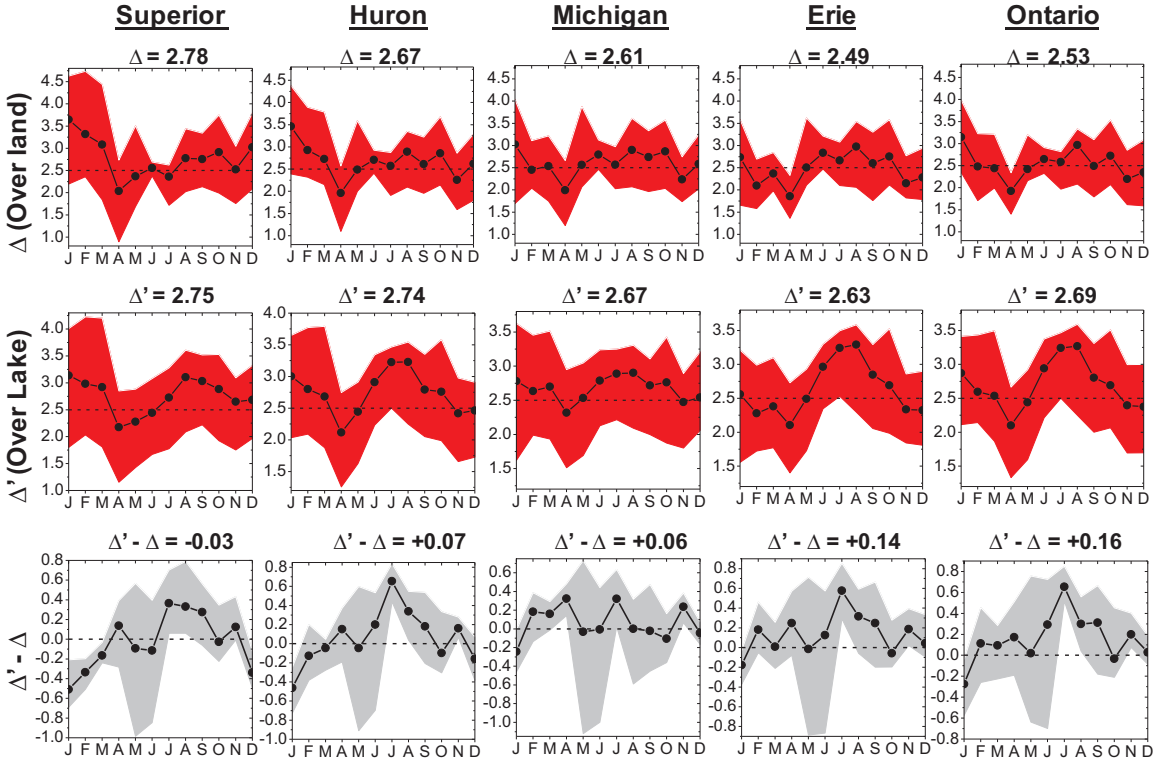

Fig. 6. Projected monthly Tmin increases in the five Great Lakes sub-basins in mid-century (2030–2059). Δ and Δ' represent the averaged air temperature Tmin changes over land and over lake relative to the baseline period (1980–2009), respectively. "Δ′ - Δ" shows the Tmin change gaps between over lake and over land.

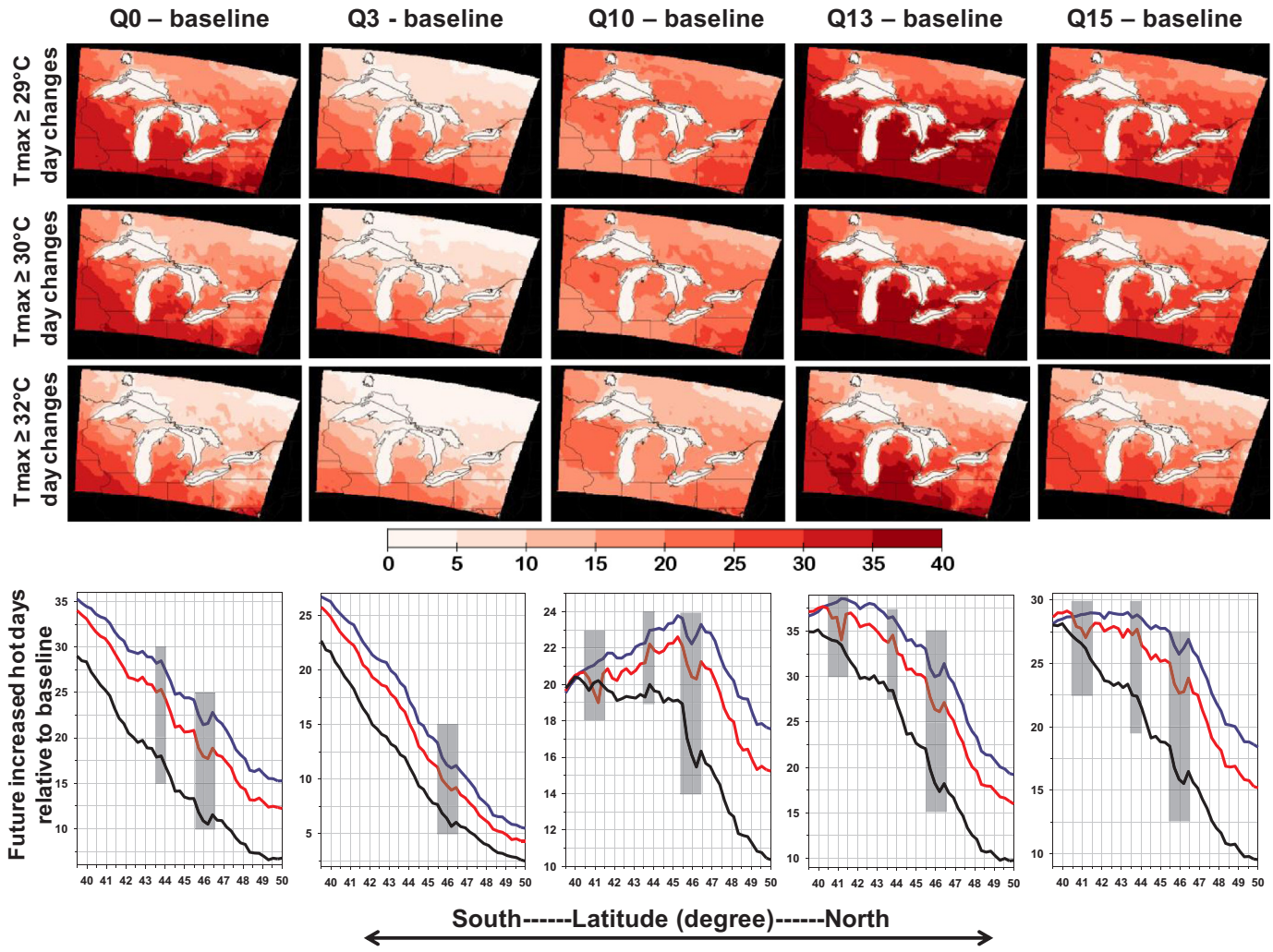

Fig. 7. Projected (2030–2059) hot (Tmax ≥ 29 °C, 30 °C, 32 °C) day changes in the area relative to the baseline period (1980–2009). Plots in the upper panel show the temporal patterns according to the 5 experiments, and the plots in the lower panel show the increase of hot days from south to north. The blue, red and black fold lines in the lower part plots represent the day changes of the day of Tmax ≥ 29 °C, 30 °C and 32 °C, respectively. Note: the dataset is narrowed within the area (north latitude 39.5–50.0°, west longitude 93.5–75.5°) to identify the Lake effects in this region, the dataset in lower figures had excluded the data over lakes, because air temperatures over lakes are very few greater than 29 °C (this means only air temperatures over land areas are calculated in lower part fold-line plots, thus it can reflect the lake effects on their adjacent land areas).

from south to north (Figs. 7 and 8), indicating these areas ("Λ" and "V" shapes) will have little converse temperature changes compared to their adjacent areas. These fluctuations in this region include the areas across the north latitude 40.5–41.5°, 43.5–44.0°, 45.5–46.5°, and 47.5–49.5° (Fig. 9). Obviously, these fluctuations of latitudinal temperature gradients in this region result from the effects of the Great Lakes, otherwise, the latitudinal temperature gradients would be smooth through south to north in this region.

Our findings (fluctuations of latitudinal temperature gradients) in this study could be compared to the temperature projection results (altitudinal and latitudinal variations) of Taiwan Island, where overland temperatures are strongly affected by ambient temperatures of adjacent ocean waters and by high inland mountains (> 3500 m) (Lin et al., 2015). These patterns highlight the strong effects of the Great Lakes on the regional climate, and again demonstrate that the models we selected are able to identify the differences between land and water areas in climate projection, which can be compared to projections of this region derived on the bases of separate land and lake climate models (Gula and Peltier, 2012; Notaro et al., 2015). To our knowledge, this may be the first report of lake-effect induced fluctuations of latitudinal temperature gradients for the region. These findings of lake-related fluctuations of latitudinal temperature gradients in the Great Lakes basin may be used in future regional agricultural management and/or even society/communities strategies adjustments response to climate change.

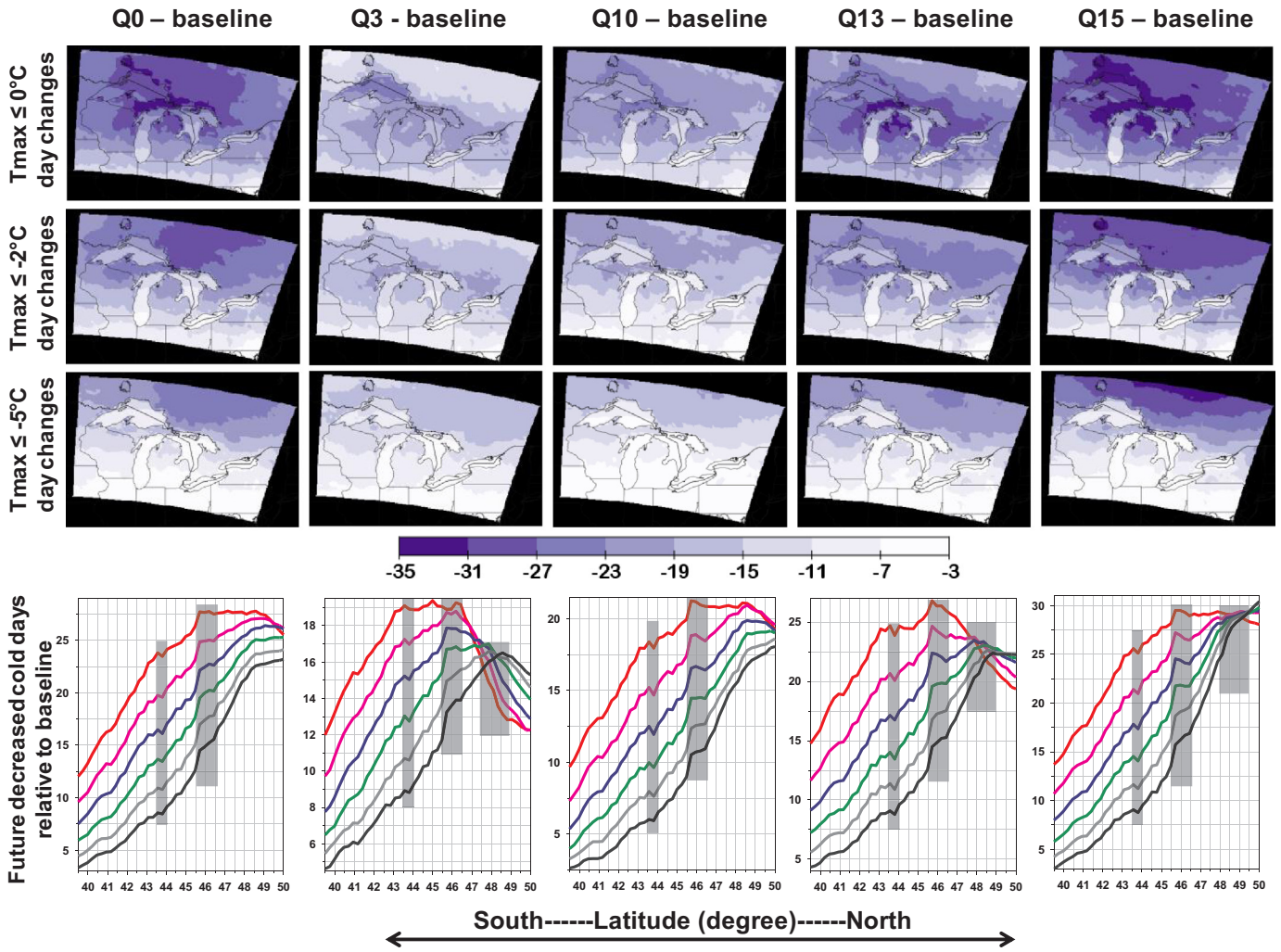

Fig. 8. Projected future (2030–2059) cold (Tmax ≤ 0 °C, −2 °C, −5 °C) day changes in the area relative to the baseline period (1980–2009). Plots in the upper panel show the temporal patterns (Tmax ≤ 0 °C, −2 °C, −5 °C) according to the 5 experiments, and plots in the lower panel show the decrease of cold days (Tmax ≤ 0 °C, −1 °C, −2 °C, −3 °C, −4 °C and −5 °C) from south to north. The red, pink, blue, green, grey and black fold lines in the lower figures represent the decreased days of Tmax ≤ 0 °C, −1 °C, −2 °C, −3 °C, −4 °C and −5 °C, respectively. Note: the dataset are narrowed within the area (north latitude 39.5–50.0°, west longitude 93.5–75.5°) to identify the Lake effects in this region. In the lower panel fold-line plots included all air temperatures dataset over lakes and lands areas, because it is common that Tmax over the basin can vary between −5 °C and + 1 °C (Scott and Huff, 1996). (For interpretation of the references to color in this figure legend, the reader is referred to the web version of this article..

4. Conclusions

In this study, we compared mid-century (2030–2059) monthly temperature changes of the Great Lakes Basin with temperatures during the baseline period (1980–2009). The results show that April and August will be the least and greatest temperature increases month in the future, respectively. Future Tmax increases in this region are likely to be greater in the interval from May to October (the growing season period) than in other months. The magnitude of future Tmax and Tmin increases will be the order: Superior > Huron > Michigan > Erie and Ontario (little fluctuation between Erie and Ontario sub-basins). Most future Tmax increases over land will be greater than those over the lakes, whereas the greatest Tmin increases are likely to occur over lakes rather than over the land areas in this region. The future number of extremely warm days (Tmax ≥ 29 °C ~ 32 °C) in this region may increase by between 5 days (north) and 40 days (south) per year, and the number of winter cold days (Tmax ≤ −5 °C ~ 0 °C) may decrease by between 3 days (south) to 35 days (north) per year. Moreover, this may be the first report of the fluctuations of latitudinal temperature gradients in the Great Lakes Basin, which include the areas across the north latitude 40.5–41.5°, 43.5–44.0°, 45.5–46.5°, and 47.5–49.5°.

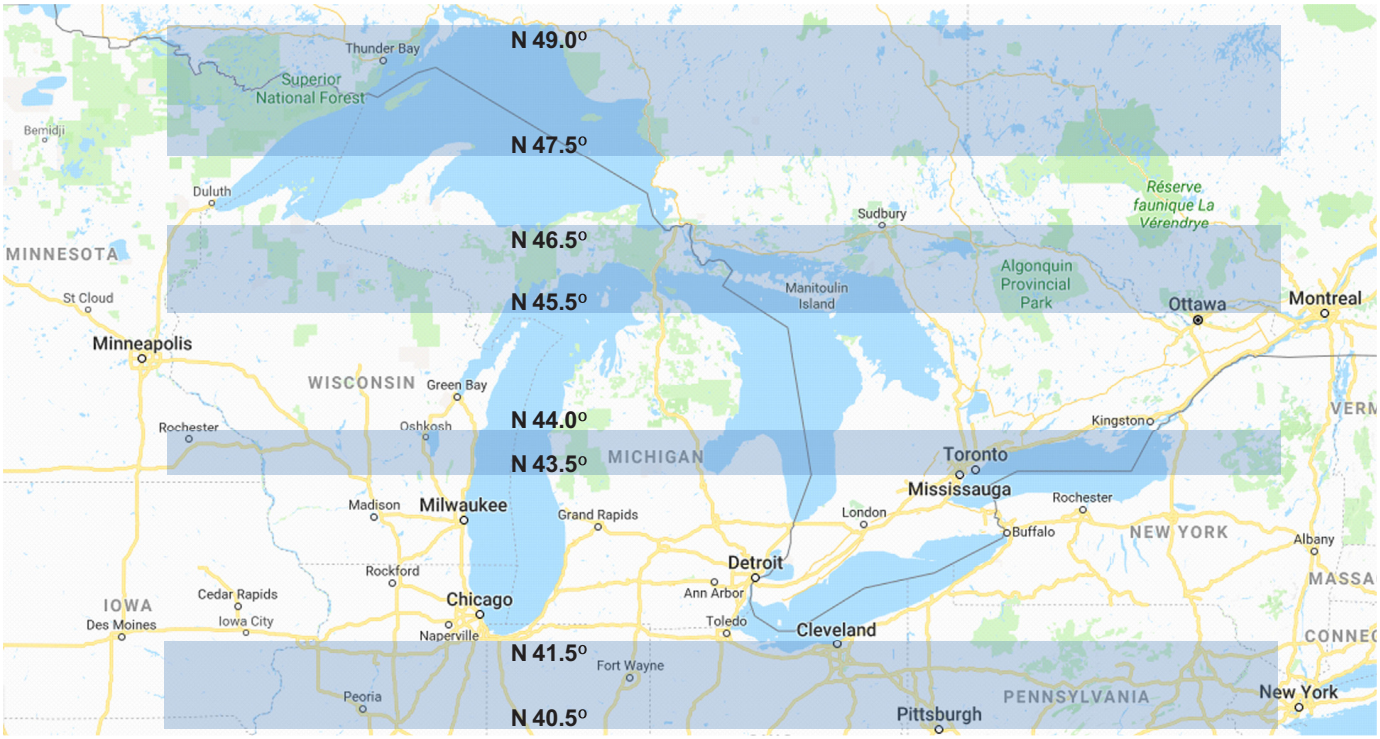

Fig. 9. The areas that present fluctuations of latitudinal temperature gradients (highlighted in grey) according to the projection results (Figs. 7 and 8) in this region.

Acknowledgments

We sincerely thank Li Wang and Mitul Chowdury for help with PRECIS data compilation. Financial support to Y Zhao was provided from Canada-Ontario Agreement Project 07-39. We extend additional thanks to the Hadley Centre for the provision of PRECIS and all GCMs input data as well as their technical support in running the model.

Funding source

Financial support to Y Zhao was provided from Ontario Ministry of Natural Resources and Forestry (Canada-Ontario Agreement) Project 07-39, Canada.

References

Andresen, J., 2017. Filed crops growing season weather summary, Michigan Agricultural Statistics 2016–2017. USDA's National Agricultural Statistics Service Michigan Field Office. Available online at: ⟨https://www.nass.usda.gov/Statistics_by_State/Michigan/Publications/Annual_Statistical_Bulletin/stats17/fieldcrops.pdf⟩.

Austin, J.A., Colman, S.M., 2007. Lake Superior summer water temperatures are increasing more rapidly than regional temperatures: a positive ice-albedo feedback. Geophys. Res. Lett. 34, L06604. https://doi.org/10.1029/2006GL029021.

Campbell, J.D., Taylor, M.A., Stephenson, T.S., Watson, R.A., Whyte, F.S., 2011. Future climate of the Caribbean from a regional climate model. Int. J. Climatol. 31, 1866–1878.

Chen, C., Lei, C., Deng, A., Qian, C., Hoogmoed, W., Zhang, W., 2011. Will higher minimum temperatures increase corn production in Northeast China? An analysis of historical data over 1965–2008. Agric. For. Meteorol. 151, 1580–1588.

Collins, M., Booth, B.B., Harris, G.R., Murphy, J.M.D., Sexton, M.H., Webb, M.J., 2006. Towards quantifying uncertainty in transient climate change. Clim. Dyn. 27, 127–147.

Constantinidou, K., Hadjinicolaou, P., Zittis, G., Lelieveld, J., 2016. Effects of climate change on the yield of winter wheat in the eastern Mediterranean and Middle East. Clim. Res. 69, 129–141.

d'Orgeville, M., Peltier, M.W., Erier, A.R., Gula, J., 2014. Climate change impacts on Great Lakes basin precipitation extremes. J. Geophys. Res. Atmos. 119, 10799–10812.

Gao, Y., Fu, J.B., Drake, Y., Liu, Y., Lamarque, J.F., 2012. Projected changes of extreme weather events in the eastern United States based on a high resolution climate modeling system. Environ. Res. Lett. 7, 044025.

Gocic, M., Trajkovic, S., 2013. Analysis of changes in meteorological variables using Mann-Kendall and Sen's slope estimator statistical tests in Serbia. Glob. Planet. Change 100, 172–182.

Gregg, R., Feifel, K., Kershner, J., Hitt J., 2012. The state of climate change adaptation in the Great Lakes region. General report. Bainbridge Is-land, WA: EcoAdapt.

Gula, J., Peltier, W.R., 2012. Dynamical downscaling over the Great Lakes basin of North America using the WRF regional climate model: the impact of the Great Lakes system on regional greenhouse warming. J. Clim. 25, 7723–7742.

Hatfield, J.L., Prueger, J.H., 2015. Temperature extremes: effect on plant growth and development. Weather Clim. Extrem. 10, 4–10.

Jones, R.G., Nouger, M., Hassell, D.C., Hassell, D., Wilson, S.S., Jenkins, G.J., Mitchell, J. F.B., 2004. Generating high resolution climate change scenarios using PRECIS. Met Office Hadley Centre Rep., 40 pp.

Kendall, M.G., 1975. Rank Correlation Methods. Griffin, London, UK.

Kling G.W., Hayhoe K., Johnson L.B., Magnuson J.J., et al. 2003. Confronting climate change in the Great Lakes Region: impacts on our communities and ecosystems, executive summary. Report of The Union of Concerned Scientists and The Ecological Society of America.

Kucharik, C., Serbin, S.P., 2008. Impacts of recent climate change on Wisconsin corn and soybean yield trends. Environ. Res. Lett. 3, 034003.

Lin, C.Y., Chua, Y.J., Sheng, Y.F., Hsu, H.H., Cheng, C.T., Lin, Y.Y., 2015. Altitudinal and latitudinal dependence of future warming in Taiwan simulated by WRF nested with ECHAM5/MPIOM. Int. J. Climatol. 35, 1800–1809.

Mann, H.B., 1945. Nonparametric tests against trend. Econometrica 13, 245–259.

Massey, N., Jones, R., Otto, F.E.L., Aina, T., Wilson, S., Murphy, J.M., Hassell, D., Yamazakif, Y.H., Allen, M.R., 2015. Weather@home-development and validation of a very large ensemble modeling system for probabilistic event attribution. Q. J. R. Meteorol. Soc. 141, 1528–1545.

McSweeney, C.F., Jones, R., Booth, B.B.B., 2012. Selecting ensemble members to provide regional climate change information. J. Clim. 25, 7100–7121.

Murphy, J.M., Sexton, D.M.H., Barnett, D.N., Jones, G.S., Webb, M.J., Collins, M., Stainforth, D.A., 2004. Quantification of modeling uncertainties in a large ensemble of climate change simulations. Nature 430, 768–772.

Neild, R.E., Newman, J.E., 1987. Growing season characteristics and requirements in the Corn Belt. National Corn Handbook. (NCH-40).

Notaro, M., Bennington, V., Lofgren, B., 2015. Dynamical downscaling–based projections of Great Lakes Water levels. J. Clim. 28, 9721–9745.

OMAFRA (Ontario Ministry of Agriculture, Food and Rural Affairs), 2016. Available online at ⟨http://www.omafra.gov.on.ca/english/environment/facts/gl_basin.htm⟩.

Sacks, W.J., Kucharik, C.J., 2011. Crop management and phenology trends in the U.S. corn Belt: impacts on yields, evapotranspiration and energy balance. Agric. For. Meteor. 151, 882–894.

Schlenker, W., Roberts, M.J., 2009. Nonlinear temperature effects indicate severe damages to US crop yields under climate change. Proc. Natl. Acad. Sci. USA 106 (37), 15594–15598.

Scott, R.W., Huff, F.A., 1996. Impacts of the Great Lakes on regional climate conditions. J. Gt. Lakes Res. 22, 845–863.

Sen, P.K., 1968. Estimates of the regression coefficient based on Kendall's tau. J. Am. Stat. Assoc. 63, 1379–1389.

Twine, T., Kucharik, E.C.J., 2009. Climate impacts on net primary productivity trends in natural and managed ecosystems of the central and eastern United States. Agric. For. Meteorol. 149, 2143–2161.

USEPA (U.S. Environmental Protection Agency), 2008. Explore our Multimedia Page. ⟨http://www.epa.gov⟩.
Vavrus, S., Van Dorn, J., 2010. Projected future temperature and precipitation extremes in Chicago. J. Gt. Lakes Res. 36, 22–32.
Wang, X., Huang, G., Baetz, B.W., 2016. Dynamically-downscaled probabilistic projections of precipitation changes: a Canadian case study. Environ. Res. 148, 86–101.
Wilson, S., Hassel, D., Hein, D., Morrell, C., Tucker, S., Jones, R., Taylor, R., 2010. Installing and using the Hadley Centre regional climate modelling system, PRECIS version 1.9.2, Met Office, Exeter, United Kingdom, 157 pp. Available online at ⟨http://precis.metoffice.com/docs/tech_man.pdf⟩.
Winslow, L.A., Read, J.S., Hansen, G.J.A., Rose, K.C., Robertson, D.M., 2017. Seasonality of change: summer warming rates do not fully represent effects of climate change on lake temperatures. Limnol. Oceanogr. 62, 2168–2178.
Wuebbles, D.J., Hayhoe, K., Parzen, J., 2010. Introduction: assessing the effects of climate change on Chicago and the Great Lakes. J. Gt. Lakes Res. 36, 1–6.
Yu, L., Zhong, S., Bian, X., Heilmanc, W.E., Andresen, J.A., 2014. Temporal and spatial variability of frost-free seasons in the Great lakes region of the United States. Int. J. Climatol. 34, 3499–3514.
Zhang, Y., Duliere, V., Mote, P.W., Salathe, E.P., 2009. Evaluation of WRF and HadRM mesoscale climate simulations over the United States Pacific Northwest. J. Clim. 22, 5511–5526.